Numerical Modeling of Nearshore Circulation on a Barred Beach with Rip Channels

K.A. Haas, I.A. Svendsen and M.C. Haller[1]

Abstract

A nearshore circulation modeling system has been applied to a closed wave basin with a longshore bar and two rip channels. The major characteristics of the flow pattern have been established by the model including the recirculation cells, the feeder currents and the bias of the rip current toward the center of the basin. Wave current interaction is established as one of the significant mechanisms in the flow. The parameters for the eddy viscosity and the bottom friction have been shown to influence the stability of the flow. The flow is generally fluctuating and large vortex systems are formed. The model results are compared with the experimental data matching magnitudes of mean velocities as well as trends of oscillations.

Introduction

The concept of rip currents was first introduced by Shepard (1936). Since then there have been many attempts to observe rip currents in the field, such as the observations by Shepard *et al.* (1941), Shepard and Inman (1951), McKenzie (1958), and Sonu (1972) to name a few. All of these studies noted that the rip currents were not steady but were transient in nature which contributed to the difficulty in obtaining accurate measurements in the field. Shepard and Inman (1951) noted that the rip current seemed to be pulsating and that eddies were being generated. Rip currents usually are described to be fed by feeder currents, although flow entrainment can be important or even dominate as described by Shepard *et al.* (1941) and McKenzie (1958).

There have also been several theoretical studies of rip currents, such as Arthur (1962) who showed that the conservation of potential vorticity requires the rip currents to become more narrow as they flow offshore. The flow across and behind

[1]Center for Applied Coastal Research, Ocean Engineering Lab, University of Delaware, Newark, DE 19716, USA. Correspondence e-mail: haas@coastal.udel.edu

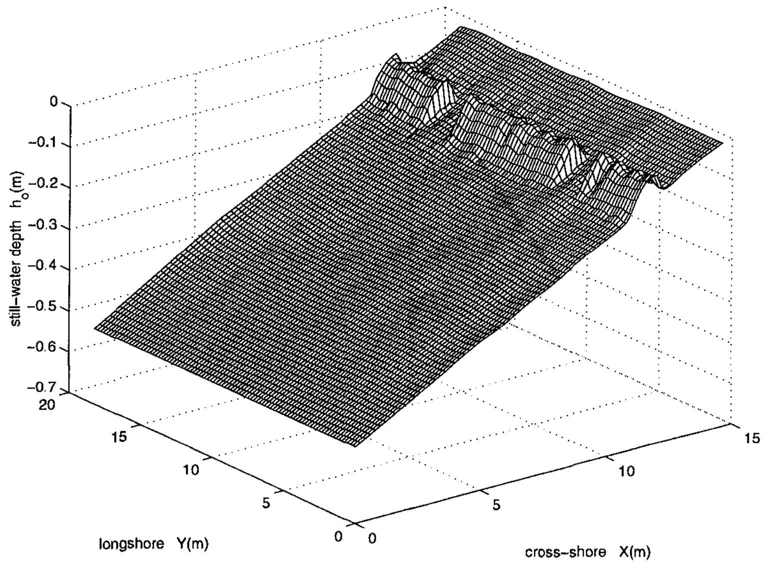

Figure 1: Bathymetry used in model simulations.

longshore bars was analyzed by Dalrymple (1978) using a simple linear model. The cross-shore flow was analyzed by the theoretical and experimental work of Svendsen and Hansen (1986) and Hansen and Svendsen (1986). These works addressed the issue of interaction between the breaking waves and circulation currents and the driving mechanisms for those currents. Computational results of a simplified version of the present model for flow over a rip channel and barred beach showed that on barred beaches with rip channels the longshore variations are important (Sancho *et al.*, 1995). Particularly, the longshore pressure gradients strongly contribute to the longshore momentum balance.

Present Problem

Dalrymple (1978) provided two classifications of the generating mechanisms for rip currents, wave interaction and structural interaction. In this study we look at rip currents in the stuctural interaction class. Specifically, we are modeling the experiment of normal incident waves in a closed wave basin with a longshore bar and two rip channels as outlined by Haller *et al.* (1997a,b). The bathymetry used in the model was taken from a detailed survey of the wave basin and is shown in figure (1). The two rip channels were intended to be symmetric to each other although they clearly have some differences. The bars also exhibit longshore non-uniformities which will have an impact on the circulation.

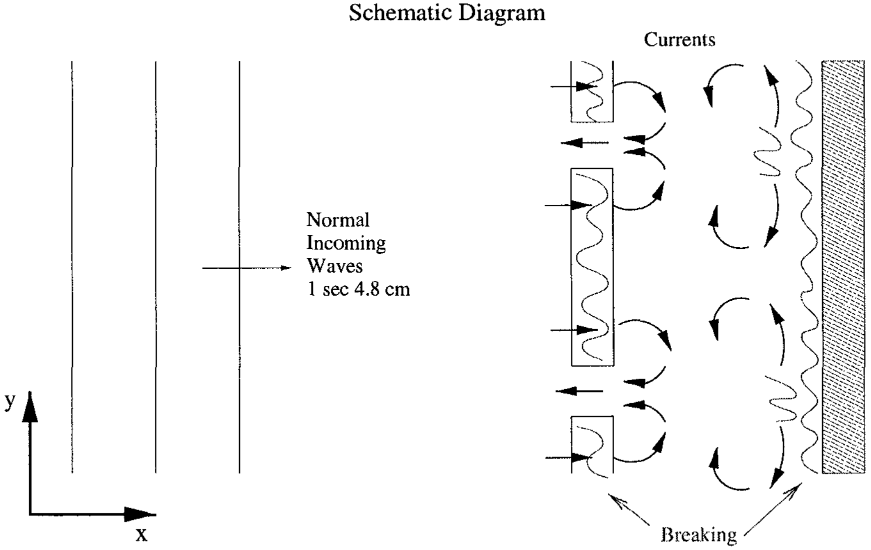

Figure 2: Schematic diagram of wave-averaged flow on a barred beach with rip channels.

Figure (2) shows a schematic diagram outlining the general flow patterns for the nearshore region of the basin. The short waves are normally incident with a period of 1 s and an off-shore wave height of 4.8 cm. These waves propagate toward the shore and start breaking over the bars, as indicated in the drawing, creating a setup in the mean water level. The waves are not breaking as much in the channels, therefore the mean water level is lower in the channels, which creates a longshore pressure gradient from the bars directed toward the channels. This pressure gradient is driving the currents towards the channels, creating the feeder currents for the rips.

Because the waves have not broken as much in the channels, these waves will be larger and therefore break earlier than the waves behind the bar as they approach the shoreline. This will create a larger setup, or a bump in the mean water level, close to the shoreline behind the channel. Therefore, a longshore pressure gradient will drive flow away from the channels creating secondary or recirculation cells close to the shoreline. Note that the circulation is highly dependent on the breaking pattern; if the waves did not break on the bar then there would be no recirculation cells and the feeder currents for the rips would be much smaller.

Model Equations

The model system is the SHORECIRC which consists of a short wave transformation component ("wave driver") and a short wave-averaged component, working simultaneously to simulate the short and long wave motions, and their interactions, in the nearshore regions. The short wave model REF/DIF (Kirby and Dalrymple, 1994) is used as the wave driver accounting for the effects of bottom induced refraction-diffraction, current induced refraction and wave breaking dissipation by solving the parabolic equation initially developed by Kirby and Dalrymple (1983).

The nearshore circulation model used is SHORECIRC, as described in Van Dongeren *et al.* (1994) and Van Dongeren and Svendsen (1997), which determines the flow pattern by solving the quasi-3D short wave-averaged hydrodynamic equations given below.

$$\frac{\partial \overline{\zeta}}{\partial t} + \frac{\partial \overline{Q}_x}{\partial x} + \frac{\partial \overline{Q}_y}{\partial y} = 0 \tag{1}$$

$$\begin{aligned}
&\frac{\partial \overline{Q}_x}{\partial t} + \rho \frac{\partial}{\partial x}\left(\frac{\overline{Q}_x^2}{h_o + \overline{\zeta}}\right) + \rho \frac{\partial}{\partial y}\left(\frac{\overline{Q}_x \overline{Q}_y}{h_o + \overline{\zeta}}\right) + \rho g \left(h_o + \overline{\zeta}\right) \frac{\partial \overline{\zeta}}{\partial x} \\
&+ \frac{\partial}{\partial x}\left(S_{xx} - \overline{\int_{-h_o}^{\zeta} \tau_{xx} dz}\right) + \frac{\partial}{\partial y}\left(S_{yx} - \overline{\int_{-h_o}^{\zeta} \tau_{yx} dz}\right) - \overline{\tau_x^S} - \overline{\tau_x^B} \\
&+ \rho \frac{\partial}{\partial x} \overline{\int_{-h_o}^{\zeta} V_{1x} V_{1x} dz} + \rho \frac{\partial}{\partial y} \overline{\int_{-h_o}^{\zeta} V_{1y} V_{1x} dz} \\
&+ \rho \frac{\partial}{\partial x} \overline{\int_{\zeta_t}^{\zeta} u_{wx} V_{1x} + u_{wx} V_{1x} dz} + \rho \frac{\partial}{\partial y} \overline{\int_{\zeta_t}^{\zeta} u_{wy} V_{1x} + u_{wx} V_{1y} dz} = 0
\end{aligned} \tag{2}$$

$$\begin{aligned}
&\frac{\partial \overline{Q}_y}{\partial t} + \rho \frac{\partial}{\partial y}\left(\frac{\overline{Q}_y^2}{h_o + \overline{\zeta}}\right) + \rho \frac{\partial}{\partial x}\left(\frac{\overline{Q}_x \overline{Q}_y}{h_o + \overline{\zeta}}\right) + \rho g \left(h_o + \overline{\zeta}\right) \frac{\partial \overline{\zeta}}{\partial y} \\
&+ \frac{\partial}{\partial x}\left(S_{xy} - \overline{\int_{-h_o}^{\zeta} \tau_{xy} dz}\right) + \frac{\partial}{\partial y}\left(S_{yy} - \overline{\int_{-h_o}^{\zeta} \tau_{yy} dz}\right) - \overline{\tau_y^S} - \overline{\tau_y^B} \\
&+ \rho \frac{\partial}{\partial x} \overline{\int_{-h_o}^{\zeta} V_{1x} V_{1y} dz} + \rho \frac{\partial}{\partial y} \overline{\int_{-h_o}^{\zeta} V_{1y} V_{1y} dz} \\
&+ \rho \frac{\partial}{\partial x} \overline{\int_{\zeta_t}^{\zeta} u_{wx} V_{1y} + u_{wy} V_{1x} dz} + \rho \frac{\partial}{\partial y} \overline{\int_{\zeta_t}^{\zeta} u_{wy} V_{1y} + u_{wy} V_{1y} dz} = 0
\end{aligned} \tag{3}$$

where x and y are the cross-shore and longshore directions, the overbar represents wave-averaging, $\overline{\zeta}$ is the mean water level, $\overline{Q_\alpha}$ is the wave-averaged volume flux in the α direction, ρ is the water density, h_o is the still water depth, $S_{\alpha\beta}$ is the radiation stress, $\tau_{\alpha\beta}$ is the turbulent stress, τ_α^S and τ_α^B are the surface and bottom shear stresses in the α direction, $V_{1\alpha}$ is the depth varying portion of the currents and $u_{w\alpha}$ is the short wave velocity. Equation (1) is the conservation of mass, equation (2) the cross-shore or x-momentum balance and equation (3) the longshore or y-momentum balance.

The first three terms in the momentum balances (equations (2) and (3)) are the local accelerations and the convective accelerations. The next term is the pressure gradient followed by the gradient of the radiation and turbulent stresses. In this study the turbulent normal stresses are neglected (i.e. the terms τ_{xx} and τ_{yy}) because they are usually considered small compared to the turbulent shear stresses. The surface shear stresses are also neglected since we are modeling a closed basin inside a laboratory. The last four terms on the left-hand side are the quasi-3D terms which act as a dispersive mixing mechanism. Traditional nearshore circulation models assume depth uniform currents which would mostly elimimate those four terms. Because this is the beginning of the study, we will also assume depth uniform currents, although, in future studies the importance of depth varying currents will be analyzed in greater detail.

The turbulent shear stresses are modeled by utilizing an eddy viscosity approach given by the following expressions, (Sancho, 1997),

$$\tau_{xy} = \rho\nu_t(\frac{\partial V_y}{\partial x} + \frac{\partial V_x}{\partial y}) \tag{4}$$

where ν_t is the eddy viscosity given by

$$\nu_t = C_1 u_o h + Mh\left(\frac{D}{\rho}\right)^{\frac{1}{3}}. \tag{5}$$

Here C_1 is a constant coefficient, u_o the bottom orbital velocity, h the total water depth, D the energy dissipation rate per unit area of the short waves, and M a constant taken to be 0.1. This eddy viscosity formulation accounts for both bottom induced and wave breaking turbulence. The first term in equation (5) represents the bottom induced turbulence which is always present and the second term represents the wave breaking turbulence which is only present in the surf zone.

The bottom shear stress is modeled using the generalized friction factor approach for waves and currents as outlined by Svendsen and Putrevu (1993),

$$\tau_\alpha^B = \frac{1}{2}\rho f_{cw} u_o(\beta_1 V_{b\alpha} + \beta_2 u_{o\alpha}) \tag{6}$$

where β_1 and β_2 are given by

$$\beta_1 = \overline{\left[\left(\frac{V_b}{u_o}\right)^2 + 2\frac{V_b}{u_o}\cos\theta\cos\mu + \cos^2\theta\right]^{\frac{1}{2}}} \tag{7}$$

$$\beta_2 = \overline{\cos\theta\left[\left(\frac{V_b}{u_o}\right)^2 + 2\frac{V_b}{u_o}\cos\theta\cos\mu + \cos^2\theta\right]^{\frac{1}{2}}}. \tag{8}$$

β_1 and β_2 are weight factors for the current and wave motion respectively and f_{cw} is the bottom friction factor.

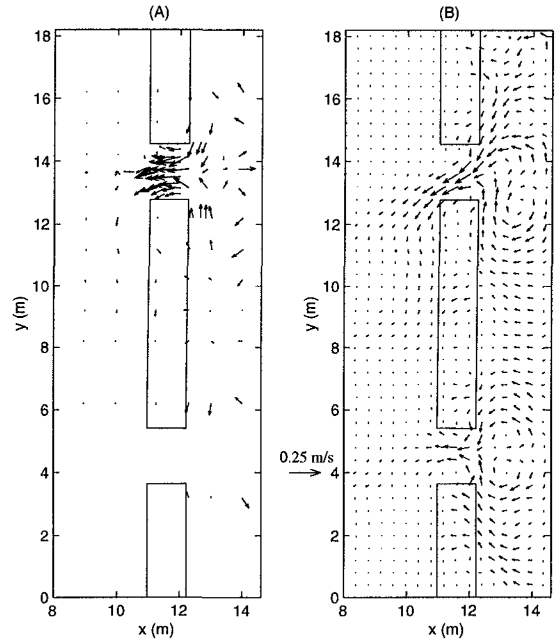

Figure 3: Time-averaged below-trough velocity vectors from (A) experimental data (described by Haller *et al.* (1997b)) and (B) SHORECIRC.

Qualitative Results

Figure (3) shows the below-trough velocity vectors for the experimental data on the left-hand side and the model results on the right-hand side. The experimental data was time-averaged for 819 seconds over the last half of the experiment. Only three velocity gauges were used at a time, however, there was a high rate of repeatability allowing all the time-averaged properties to be examined simultaneously. The model results were time-averaged over 750 seconds after beginning from a cold start for 200 seconds. The model data results from a single model run in which the velocities were the qualitative best fit with the experimental data.

The majority of the experimental data is gathered around the upper rip channel so we will primarily focus on the flow around that rip channel. The rip currents are easily identifiable in the channels for both the experiment and model. In both diagrams of figure (3), the rip currents vanish just seaward of the channel. The rips are also biased toward the center of the basin in both the experiment and the model. The flow leaving the rip channel in the model turns toward the center of the basin and flows back onto the bar and then runs shore parallel, similar to the experimental results. The magnitude of the rip currents in the channel also are similar. The rip in the model has flow entrainment which causes the rip to widen offshore. The model from Arthur (1962) predicts that the rips should become narrower but that model does not allow for flow entrainment.

The recirculation cells discussed earlier are clearly evident in both the experimental and the model results. However, the experiment shows a stronger shoreward flow behind the channel close to the shoreline, which is not present in the model results. This will be discussed in greater detail later. The two recirculation cells for the upper rip in the model are unequal due to the irregularities in the bathymetry previously mentioned. The flow around the two rip channels also exhibit many differences which is a result of the seemingly minor differences in the bathymetry of the channels. We also noticed that the feeder currents are similar between the two figures with the upper feeder currents being at a slight angle toward the channel and the lower feeder currents being shore parallel. The magnitude of the currents behind the bar are similar between the two cases.

Wave Current Interaction

The wave current interaction is accounted for in the model system and proves to be an important mechanism, particularly around the strong rip currents. The governing equation in REF/DIF accounts for the effect of large currents including the doppler shift due to currents.

The wave current interaction is modeled interactively by initially determining the short waves without currents and then calculating the resulting currents with SHORECIRC. The currents and mean water level are fed back into REF/DIF to determine the new wave field. This process is constantly repeated to provide for the wave current interaction. In the present study the short waves are calculated approximately once every short wave period. The wave field, and therefore the forcing, only has small changes over this short time scale, providing smooth transitions between the different forcings.

The effect of including the wave current interaction is shown in figures (4), (5) and (6). Figure (4) shows the cross-shore sections of the short wave height across the center bar and through the channel for cases with and without wave current interaction. In general, the waves over the bar shoal and break on the bar (as indicated by the steep decline in wave height), then reform, shoal and break at the shoreline. On the other hand, the waves in the channel only have a single break point and, therefore, tend to start breaking earlier as they approach the shoreline. We see that inclusion of the currents causes the wave heights in the channel to increase slightly and the onset of breaking occurs farther offshore in the channel. The comparisons with experimental data shows that these trends, if not the exact magnitudes, are matched. It is more important to match the gradient of the wave heights because the forcing is due to the gradient of the radiation stresses which is proportional to the gradient of the wave height.

Figure (5) shows the mean water level for the same two cross-shore sections with

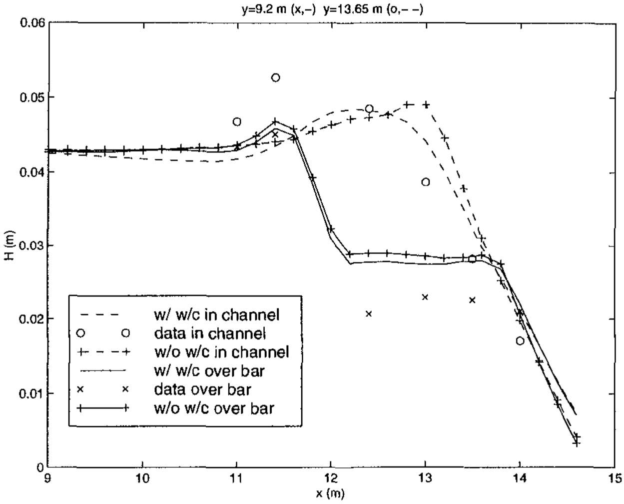

Figure 4: Comparison of time-averaged modeled short-wave height with and without wave current (w/c) interaction to experimental data (described by Haller *et al.* (1997b)).

and without wave current interaction again. The longshore pressure gradient between the channel and the bar is evident between $x = 12 - 13.5$ m. This longshore pressure gradient is reversed, although much smaller, closer to the shoreline. The effect of the wave current interaction on the mean water level is most evident in the channel around $x = 12 - 13.5$ m where the water level is significantly reduced. Everywhere else the differences appear to be insignificant. In particular, the changes along the center of the channel due to the currents turn out to be important, even though they may appear small. However, it is emphasized that although the sine wave theory of REF/DIF has been modified, it does not model the forcing of breaking waves accurately.

Finally, figure (6) shows the vorticity and below trough velocity vectors demonstrating the most significant impact of the wave current interaction on the circulation pattern. The most significant change is that with the wave current interaction included, the rip current does not extend very far offshore of the channel and is biased toward the center of the basin. The recirculation cells are smaller and do not extend over the bar as they do for the case without wave current interaction. The experimental data in figure (3) also shows that the rip vanishes and is biased toward the center of the basin. We have found that this effect is only achieved in the model if we include the wave current interaction.

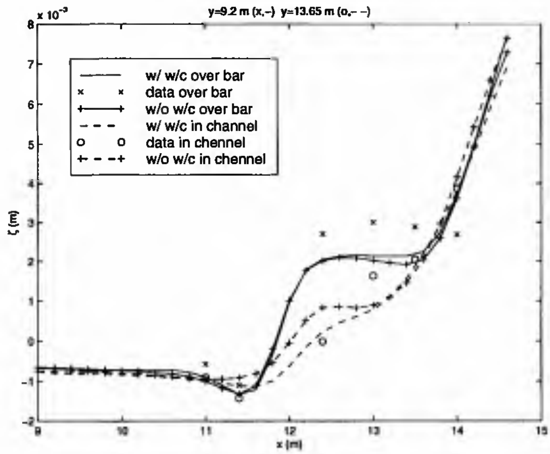

Figure 5: Comparison of time-averaged modeled mean water level with and without wave current (w/c) interaction to experimental data (described by Haller *et al.* (1997b)).

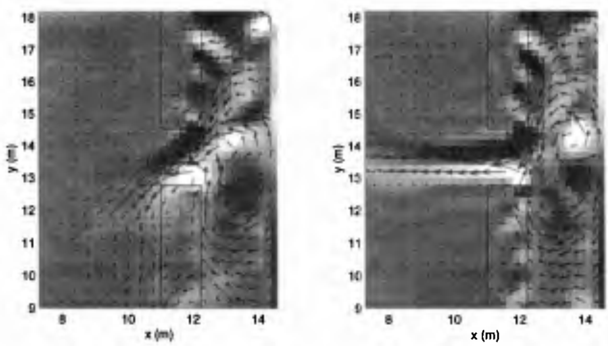

Figure 6: Below trough time-averaged velocity vectors with vorticity contours. The left side is with wave current interaction and right side is without wave current interaction. White contours are positive vorticity and black contours are negative vorticity.

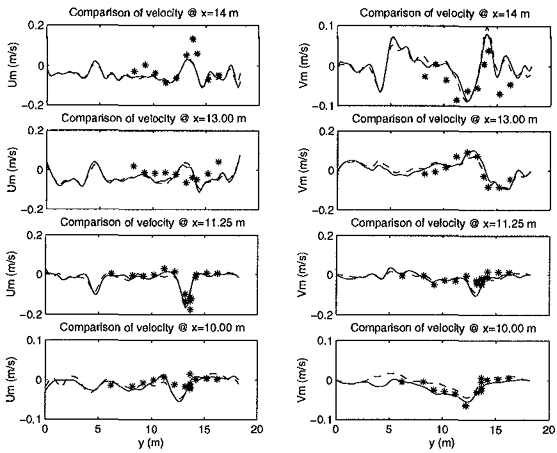

Figure 7: Comparison of time-averaged below-trough velocity for cross-shore (Um) and longshore (Vm) flow with experimental data (described by Haller *et al.* (1997b)). Solid line (-) is for $C_1 = 0.001$, dashed line (- -) is for $C_1 = 0.01$ and asterix (*) is the experimental data.

Selection of Parameters

The important flow parameters which have been adjusted to fit the experimental data are the eddy viscosity coefficient (C_1) and the bottom friction factor (f_w). The parameter C_1 is varied between 0.001 and 0.01. This parameter will change the eddy viscosity due to the bottom induced turbulence. Therefore, changing the parameter will primarily affect the flow outside the surfzone because the term representing breaking wave conditions will dominate inside the surfzone. The friction factor is estimated from Jonsson (1966) and has a range from 0.01 to 0.035 accounting for the uncertainty in bottom roughness and the variable flow conditions.

Figure (7) shows velocity profiles for longshore sections at four cross-shore locations; moving down, at the shoreline ($x = 14$ m), in the trough ($x = 13$ m), over the bar ($x = 11.25$ m) and seaward of the bar ($x = 10$ m). This figure shows two cases with an eddy viscosity coefficient, C_1, of 0.001 and 0.01 and the friction factor being held constant at $f_w = 0.03$. The most significant change occurs in the longshore velocity offshore of the bar, where the velocity for the higher eddy viscosity is slightly reduced. The increased eddy viscosity tends to help stabilize the flow, therefore significantly reducing the meandering of the rip current. Less meandering of the rip current will produce less time-averaged longshore velocity in the rip.

Figure (8) shows velocity profiles of the same longshore sections for $f_w = 0.015$ and $f_w = 0.03$ and C_1 being held constant at 0.001. The variation between the two

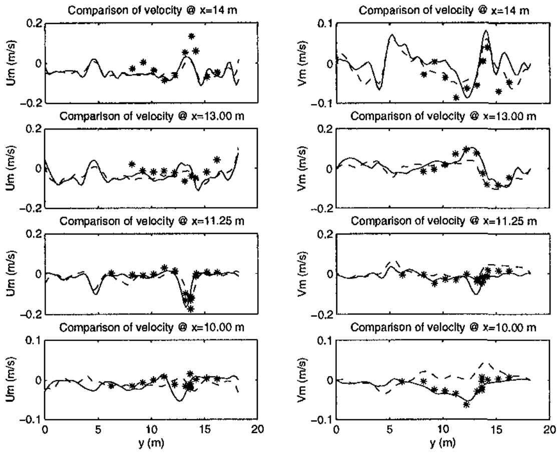

Figure 8: Comparison of time-averaged below-trough velocity for cross-shore (Um) and longshore (Vm) flow with experimental data (described by Haller *et al.* (1997b)). Solid line (-) is for $f_w = 0.03$, dashed line (- -) is for $f_w = 0.015$ and asterix (*) is the experimental data.

cases is much more significant. As with the eddy viscosity, increasing the bottom friction tends to stabilize the flow. The time-averaged cross-shore velocity in the rip current tends to be larger for higher friction factors because less meandering of the current produces less mixing. The longshore velocity for the lower friction case for the farthest offshore sections tends to be antisymmetric (i.e. the current is positive on one side of the rip channel and negative on the other), whereas the higher friction tends to have the longshore current in one direction. The lower friction factor allows the rip to meander fairly equally in both directions whereas the higher friction factor, and experimental data, shows a bias toward the inside of the basin. Even though the higher friction case has smaller instantaneous velocities, the time-averaged velocities in the rip are higher because the flow is more stable with less mixing.

Multiple cases for the range of the eddy viscosity coefficient, C_1 between 0.001 and 0.01, and the bottom friction factor, between $f_w = 0.015$ and 0.03 were run to obtain the best fit with the experiments. From these different cases the best visual match of the currents with the experimental data was selected. The parameters that best fit the data turned out to be $C_1 = 0.001$ and $f_w = 0.03$. These are the same parameters used for the model results in figure (3). The relatively high f_w is in conjuction with the small scale experiment where the boundary layer is in the laminar-turbulent transition region. Figure (9) shows the currents for the final selection of parameters for cases with and without wave current interaction in the same longshore sections as figures (7) and (8). This figure demonstrates that the inclusion of the wave current interaction improved match with the measured data, particularly the flow around the rips.

Close to the shoreline, the top panels in figure (9), the cross-shore velocity is too small and the longshore velocity is too large. This is probably a result of the recirculation cells in the model being shifted seaward relative to the experiments because the shoreline boundary condition is a wall with an average still water depth around 6 mm. Presumably, utilizing a moving shoreline condition could improve the match with data close to the shoreline. The recirculation cells being shifted seaward could also explain why the cross-shore velocity in the trough (second panel on the left) is less accurately predicted.

Some of the inaccuracies around the rip channels and in the trough region between the bar and the shoreline could be a result of incorrect breaking patterns. The short wave driver uses a bottom induced breaking criteria which causes the waves in the channel to break closer to the shoreline. Visual observation of the experiments showed that the waves in the channels were breaking somewhat earlier due to the increased short wave steepness from the oppossing current. Correctly predicting the breaking pattern and the forcing due to the breaking waves would also improve the comparison with the data, although, in general, the magnitudes of the currents from the model match fairly well with the experimental data.

Finally it may be noticed that only the time-averaged properties of the flow field are presented here because they provide the best means of comparison with the experiments. The time varying properties of the currents and mean water level show many similarities with the experiments. The flow for both cases is unstable. The rip has instabilities on several time scales, typically a faster scale ~ 20 seconds, which appears to be related to the instability of a jet and slower motions with scales $\sim 100 - 300$ seconds. The experiments (Haller *et al.*, 1997b) have shown similar trends. The model also shows eddies being created and shed from the rips as well as from the flow behind the bar. The time series from the experiments show some evidence of eddies passing through the sensors in a similar fashion.

Conclusions

A study on rip currents has been performed by applying a numerical nearshore circulation model system to an experiment in a closed wave basin with a barred beach containing two rip channels. The breaking pattern resulting from this bathymetry has been identified to be an important driving mechanism of the nearshore currents. Significant changes occur when the wave current interaction is included in the model system such as the rip current vanishing quickly offshore and being biased toward one side as is also found in the experiments. In general, the model and experiments are in agreement.

The effect of several flow parameters has been analyzed including the eddy viscosity and the bottom stress. Both parameters are a factor in controlling the stability of the flow. Decreasing either parameter causes the flow to become more unstable. These parameters can be varied to give a qualitative best fit of the modeled cur-

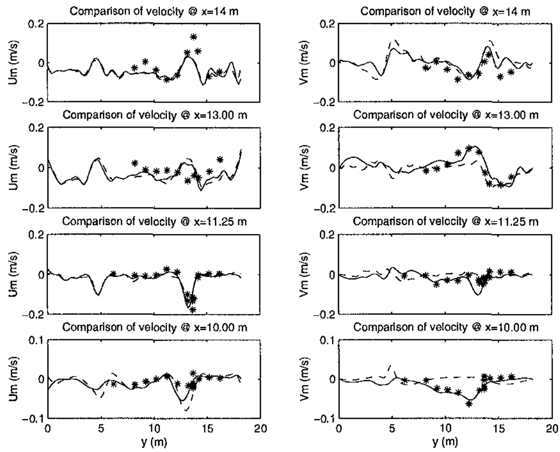

Figure 9: Comparison of time-averaged below-trough velocity for cross-shore (Um) and longshore (Vm) flow with experimental data (described by Haller *et al.* (1997b)). Solid line (-) is with wave current interaction, dashed line (- -) is without wave current interaction and asterix (*) is the experimental data.

rents to the experimental data. Changes in the eddy viscosity does not produce large changes in the flow pattern. Variations in the bottom stress are more important. The values of the two coefficients selected for matching the experimental data are physically realistic. Currents have been assumed depth uniform in this preliminary study.

Acknowledgements

This work was sponsored by Sea Grant, under Award No NA56 NG 0147 and by ONR (contract no N00014-95-C-0075). The US government is authorized to produce and distribute reprints for government purposes non withstanding any copyright notation that may appear herein.

References

Arthur, R. S. (1962). A note on the dynamics of rip currents. *Journal of Geophysical Research*, **67**, 2777–2779.

Dalrymple, R. A. (1978). Rip currents and their causes. In *Proceedings of the 14th Coastal Engineering Conference*, pages 1414–1427.

Haller, M., Dalrymple, R., and Svendsen, I. (1997a). Rip channels and nearshore circulation: Experiments. In *Proceedings Coastal Dynamics*.

Haller, M., Dalrymple, R., and Svendsen, I. (1997b). Experimental modeling of a rip current system. In *Proceedings of the Third International Symposium on Ocean Wave Measurement and Analysis*.

Hansen, J. and Svendsen, I. A. (1986). Experimental investigation of the wave and current motion over a longshore bar. In *Proceedings of the 20th Coastal Engineering Conference*, pages 1166–1179.

Jonsson, I. G. (1966). Wave boundary layers and friction factors. In *Proceedings of the 10th Coastal Engineering Conference*, volume 1, pages 127–148, Tokyo. ASCE.

Kirby, J. and Dalrymple, R. (1994). Combined refraction/diffraction model ref/dif 1, version 2.5. Technical Report CACR-94-22, Center for Applied Coastal Research, University of Delaware.

Kirby, J. T. and Dalrymple, R. A. (1983). A parabolic equation for the combined refraction-diffraction of stokes waves by mildly varying topography. *Journal of Fluid Mechanics*, **136**, 453–466.

McKenzie, P. (1958). Rip current systems. *Journal of Geology*, **66**, 103–113.

Sancho, F. (1997). *Unsteady Nearshore Currents on Longshore Varying Topographies*. Ph.D. thesis, University of Delaware.

Sancho, F., Svendsen, I., Van Dongeren, A., and Putrevu, U. (1995). Longshore nonuniformities of nearshore currents. In *Proceedings Coastal Dynamics*, pages 425–436.

Shepard, F. P. (1936). Undertow, rip tide or rip current. *Science*, **84**, 181–182.

Shepard, F. P. and Inman, D. L. (1951). Nearshore circulation. In *Proceedings of the 1st Coastal Engineering Conference*, pages 50–59.

Shepard, F. P., Emery, K. O., and La Fond, E. (1941). Rip currents: a process of geological importance. *Journal of Geology*, **49**, 337–369.

Sonu, C. J. (1972). Field observations of nearshore circulation and meandering currents. *Journal of Geophysical Research*, **77**, 3232–3247.

Svendsen, I. A. and Hansen, J. B. (1986). The interaction of waves and currents over a longshore bar. In *Proceedings of the 20th Coastal Engineering Conference*, pages 1580–1594.

Svendsen, I. A. and Putrevu, U. (1993). Surf zone wave parameters from experimental data. *Coastal Engineering*, **19**, 283–310.

Van Dongeren, A., Sancho, F., Svendsen, I., and Putrevu, U. (1994). Shorecirc: A quasi-3d nearshore model. In *Proceedings of the 24th Coastal Engineering Conference*, pages 2741–2754.

Van Dongeren, A. R. and Svendsen, I. A. (1997). Quasi-3D modeling of nearshore hydrodynamics. (Ph. D. Dissertation), Res. Report CACR-97-04, Center for Applied Coastal Research, Univ. of Delaware.